Coherent Coupling of Multiple Transverse Modes in Quantum Cascade Lasers

Nanfang Yu,[1] Laurent Diehl,[1] Ertugrul Cubukcu,[1] David Bour,[2] Scott Corzine,[2] Gloria Höfler,[2] Aleksander K. Wojcik,[3] Kenneth B. Crozier,[1] Alexey Belyanin,[3,*] and Federico Capasso[1,*]

[1]*School of Engineering and Applied Sciences, Harvard University, Cambridge, Massachusetts 02138, USA*
[2]*Agilent Laboratories, 3500 Deer Creek Road, Palo Alto, California 94304, USA*
[3]*Department of Physics, Texas A&M University, College Station, Texas 77843, USA*

(Received 21 February 2008; published 5 January 2009)

Quantum cascade lasers are a unique laboratory for studying nonlinear laser dynamics because of their high intracavity intensity, strong intersubband optical nonlinearity, and an unusual combination of relaxation time scales. Here we investigate the nonlinear coupling between the transverse modes of quantum cascade lasers. We present evidence for stable phase coherence of multiple transverse modes over a large range of injection currents. We explain the phase coherence by a four-wave mixing interaction originating from the strong optical nonlinearity of the gain transition. The phase-locking conditions predicted by theory are supported by spectral data and both near- and far-field mode measurements.

DOI: 10.1103/PhysRevLett.102.013901 PACS numbers: 42.60.Fc, 42.25.Kb, 42.55.Px, 42.60.Jf

Quantum cascade lasers (QCLs) boast a combination of nonlinear dynamic properties that is unique among solid-state lasers. On one hand, an ultrafast (~1 ps) electron relaxation time in excited subbands and an even faster relaxation of the intersubband coherence make QCLs the only solid-state lasers belonging to the group of class-A lasers [1], in which population inversion and polarization adiabatically follow the dynamics of the electromagnetic field. On the other hand, a very large dipole moment of the intersubband transitions in combination with high intracavity intensity gives rise to a large Rabi frequency of the order of 1 THz. Therefore, one can expect that nonlinear effects originating from spectral and spatial hole burning that are only marginal or nonexistent in other types of semiconductor lasers will be ubiquitous in QCLs. Indeed, in recent papers [2,3], we reported observations of multi-longitudinal-mode instabilities including the coherent Risken-Nummedal-Graham-Haken (RNGH) instability in different types of QCLs. In this Letter we present evidence that the nonlinear coupling between the transverse modes of a QCL is equally ubiquitous and gives rise to strong phase coherence effects.

Experimental evidence for beam steering has been recently reported in the far field of high power QCLs and explained by interference of the two lowest order transverse modes [4]. Previously, similar phenomena were observed in diode lasers and also explained as transverse-mode frequency and phase locking; see, e.g., [5–10], and references therein. However, most of the above works dealt with diode lasers and considered only two-mode coupling. The salient features of diode lasers and, in particular, the mechanisms of phase locking are quite different from the relevant properties of QCLs. In diode lasers, the locking is primarily due to density modulation of free carriers, which is proportional to the linewidth enhancement factor α. In QCLs the total electron density is not affected by the laser field and the α factor is negligible. In this case the mode coupling is due to gain saturation and the concomitant strong spatial hole burning, which favors multimode operation [2,3].

In this Letter, we perform systematic spectral, near-field and far-field transverse-mode measurements of QCLs. We observe phase coherence between multiple transverse modes and explain it by a four-wave mixing interaction. We find that the condition of phase locking is in good agreement with the prediction of the theory.

Buried heterostructure QCLs ($\lambda \approx 7\ \mu$m) [11] with the same quantum well design but different ridge width (8, 12, 17, and 22 μm) were employed in these measurements. A minimum of two devices for each ridge width was studied. Except for the 8 μm wide QCLs, which were too narrow to operate on more than one transverse mode, all lasers showed clear and consistent evidence of phase locking of multiple transverse modes. In the present Letter, we focus on the results obtained with lasers of two different active region width: 12 and 22 μm. High-resolution laser spectra (resolution 0.125 cm^{-1}) of the 12-μm devices show that there is more than one set of longitudinal modes [Fig. 1(a)], indicating excitation of several transverse modes. A Fourier analysis of this spectrum reveals three closely

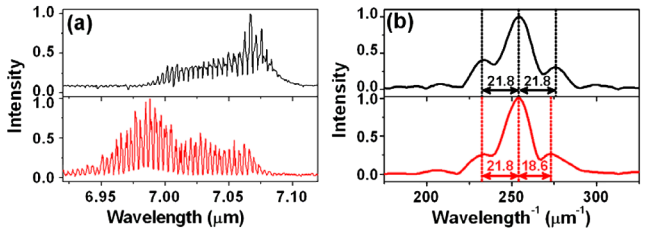

FIG. 1 (color online). (a) Spectra of a QCL with a 12-μm-wide active region. (b) Fourier transform of the spectra. The laser is driven by pulsed current $I = 1.0$ A (upper panel) and 0.75 A (lower panel) at a repetition rate of 80 kHz. The pulse duration is 125 ns.

spaced peaks [Fig. 1(b)]. It is natural to attribute them to three combs of longitudinal modes belonging to three dominant transverse modes with slightly different effective refractive indices. Similar spectra were observed for lasers with a broad 22-μm active region.

QCL far-field mode profiles were measured using a setup that is based on a rotation stage. Near-field mode profiles were characterized by a midinfrared apertureless near-field scanning optical microscope (mid-ir a-NSOM) [12]. In the experiment, a metal coated atomic force microscope tip oscillates at frequency f_o and scans the laser facet, scattering the near field of the laser mode into the far field. We demodulated the detected scattered light at $2f_o$, in order to discriminate the scattered near field from the background [12]. In order to enhance detection sensitivity, the interference between the near field scattered by the tip apex and the direct laser output is detected, and the NSOM image is a map of the amplitude of the near field of the transverse mode [12,13].

The measured far-field and near-field mode profiles for two sets of devices with widely different ridge widths (12 and 22 μm) show clear evidence of coherent coupling of multiple transverse modes [Figs. 2(b), 3, 4(b), and 5]. To extract information of the constituent transverse modes from the measured mode profiles, we first perform simulations to solve the transverse eigenmodes of the QCL waveguide. Then a near-field mode profile is expressed as a combination of several transverse eigenmodes including their relative amplitudes and phases. A Fresnel diffraction integral is then used to calculate the corresponding far-field mode profile. By fitting it to the experimental far-field profiles, we find that there are three constituent transverse modes with specific phase and amplitude relations [Figs. 2(c) and 4(c)]. The far-field fits are quite sensitive to small changes of the phases and amplitudes of the constituent transverse modes. In order to quantify this, we use error bars in Figs. 2(c) and 4(c) to indicate the range of individual parameter changes that could lead to a root mean square deviation of 0.05 between the experimental data and the fits. We note that under small driving current conditions, we cannot reliably determine the amplitudes and phases of the two weak transverse modes. The uncertainty of fitting parameters for small current conditions therefore is large [Figs. 2(c) and 4(c)]. However, the small current regime is not of interest to us; our study focuses on laser operation at sufficiently large currents when the intensity of the three modes is high enough to ensure strong nonlinear coupling.

As an independent check of the reliability of the far-field fits, we plot the experimental a-NSOM near-field mode profiles together with the near-field profiles obtained using the correct parameters determined from far-field fits. We find a reasonably good agreement between the two [Figs. 3(b) and 5(b)]: the coefficient of determination R^2 for the near-field fits was found to be about 0.95 for the 12-μm wide device and about 0.90 for the 22-μm wide device. The correlated far-field and near-field measure-

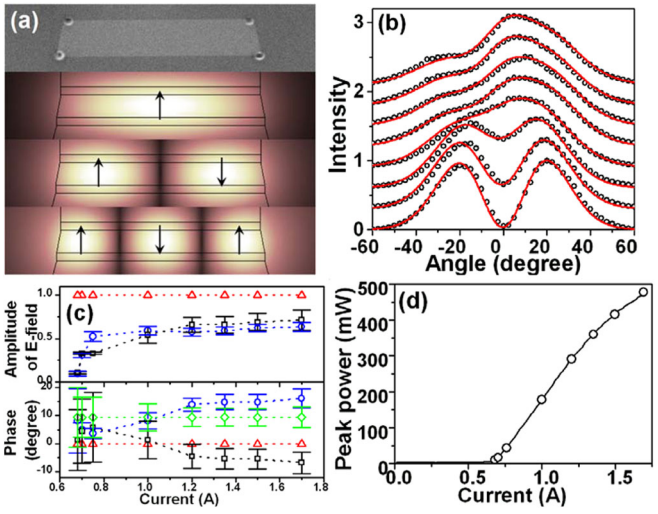

FIG. 2 (color online). (a) SEM image of the facet of a QCL with a 12-μm-wide active region, and simulations showing from top to bottom the electric field of TM_{00}, TM_{01}, and TM_{02} modes for the device; the arrows in the figure indicate the polarization of the field. (b) Measured far-field intensity distributions of the device (open circles) and their fits (solid lines) at driving currents of 1.7, 1.5, 1.35, 1.2, 1, 0.75, 0.70, and 0.68 A (from top to bottom). The curves are shifted vertically for clarity. (c) Electric-field amplitude (upper panel) and phase (lower panel) of the transverse modes used to fit the far-field data in (b). Open circles: TM_{00} mode; open triangle: TM_{01} mode; open squares: TM_{02} mode; open diamonds: $\phi_{TM00} + \phi_{TM02} - 2\phi_{TM01}$. Dotted lines are used to guide the eyes. Error bars indicate the range of individual parameter changes that will lead to a root mean square deviation of 0.05 between the experimental data and the fits. (d) Light output versus current (LI) curve for the device. The LI curve is free of kinks, indicating a smooth growth of all the mode components. The dots indicate the operating conditions at which the near- and far-field measurements were performed.

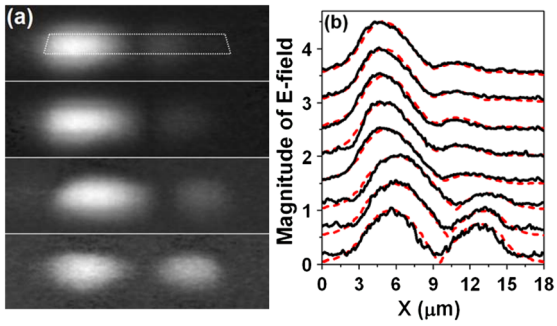

FIG. 3 (color online). (a) NSOM images of the laser modes on the facet of the 12-μm QCL at driving currents of 1.7, 1.0, 0.75, and 0.68 A (from top to bottom). Image size: 18 μm $\times$ 5 μm. The dashed trapezoidal frame in the first panel indicates the laser active region. (b) Line scans of the NSOM images (solid lines) and near-field mode profiles (dashed line) calculated using the amplitudes and phases extracted from the far-field fits [Fig. 2(c)] at driving currents of 1.7, 1.5, 1.35, 1.2, 1, 0.75, 0.70, and 0.68 A (from top to bottom). The near-field mode profiles are shifted vertically for clarity.

ment results form solid experimental evidence of phase locking.

We propose the following simple model of phase coherence between transverse modes. In the presence of a Fabry-Perot laser cavity, each transverse mode of a waveguide consists of a comb of longitudinal cavity modes. At low laser intensities, longitudinal modes belonging to different transverse modes are uncorrelated. At high intensities, however, these longitudinal modes become coupled due to four-wave mixing mediated by the saturation nonlinearity of the laser transition. We show that the latter process leads to the frequency and phase locking between longitudinal modes belonging to different combs. Our theory predicts definite values for the relative amplitudes, frequencies, and phases of locked modes that turn out to be in excellent agreement with observations.

Note that there is no contradiction with the known result stating that four-wave mixing of longitudinal modes in the two-level active region alone cannot lead to a stable phase-locking [1]. This result is not applicable when interacting longitudinal modes belong to different transverse modes. Feasibility of a stable phase locking for two transverse modes was shown, e.g., in Ref. [4] as well as in Ref. [10] and Refs. [1–5] therein. However, the modal frequencies have to be locked to the same values. This is not the case with our lasers where multiple transverse modes at different frequencies are clearly distinguishable in the spectra.

We start from standard Maxwell-Bloch equations [1,2] in which the electric field in a laser cavity is expanded into a series over a set of the cavity modes $E_i(\mathbf{r})$: $\mathbf{e}(\mathbf{r}, t) = \sum \frac{1}{2} a_i(t) \exp(-i\omega_0 t) E_i(\mathbf{r}) + \text{c.c.}$, where ω_0 is a central frequency of the laser transition. Since relaxation times $T_1 \sim 1$ ps and $T_2 \sim 0.1$ ps of the population inversion N and the coherence ρ_{21} (i.e., the off-diagonal element of the density matrix) of the laser transition are much shorter than the photon lifetime ~ 10 ps, we can adiabatically eliminate N and ρ_{21} and arrive at the equations for the field amplitudes in the $\chi^{(3)}$ approximation:

$$da_j/dt + (\alpha_j + i(\omega_{cj} - \omega_0))a_j = \frac{g_j}{2}\left\{\sum_k a_k \int_{AR} \varepsilon E_j E_k dV - \frac{1}{I_s}\sum_{k,l,m} G_{jklm} a_k (a_l^* a_m + a_l a_m^*)\right\}, \quad (1)$$

where the overlap integrals $G_{jklm} = \int_{AR} \varepsilon E_j E_k E_l E_m dV$ over the active region volume are calculated numerically, $g_j = 4\pi\omega_0 d^2 N_p T_2/(\hbar\mu_j^2)$ is the small-signal material gain, μ_j the effective refractive index of the jth mode, $I_s = 2\hbar^2/(d^2 T_1 T_2)$ the saturation intensity, ω_{cj} and α_j are the frequency and the modal loss of the jth "cold" mode, d the dipole moment of the laser transition, and N_p the population inversion supported by pumping in the absence of laser generation. Here cold denotes modal parameters calculated assuming no interaction between modes.

The second term on the right-hand side of Eq. (1) describes the phase-sensitive nonlinear coupling between different modes which can lead to their frequency and phase locking. Since our lasers have three transverse modes involved in generation, we divide the whole spectrum of three overlapping combs into triplets of longitudinal modes, with each mode in the triplet belonging to a different transverse mode 1, 2, or 3, and consider the four-wave mixing process $j + j \leftrightarrow k + l$ within each triplet. We express the complex amplitude of each longitudinal mode via its real amplitude and phase as $a_j(t) = f_j(t) \times \exp(i\varphi_j(t) - i\Delta_j t)$, where $\Delta_j = \omega_j - \omega_0$ is the detuning of the frequency of a jth "hot" mode from the transition frequency. Here hot denotes actual (unknown) frequencies, phases, and amplitudes of laser modes with the nonlinear interaction taken into account. Then Eq. (1) yields six equations with real coefficients for the amplitudes and phases of these modes. For 12-μm wide lasers, three transverse modes 1, 2, and 3 are TM_{00}, TM_{01}, and TM_{02} modes, respectively. We find that the process that can lead to phase locking is of the type $TM_{01} + TM_{01} \leftrightarrow TM_{00} + TM_{02}$, which corresponds to the phase combination $2\varphi_2 - \varphi_1 - \varphi_3$:

$$\begin{aligned} d(2\varphi_2 - \varphi_1 - \varphi_3)/dt + \delta_1 + \delta_3 - 2\delta_2 \approx -(g/I_s)\{&G_{1122}(2f_1^2 + f_2^2)\sin 2\Phi_{12} + G_{2233}(2f_3^2 + f_2^2)\sin 2\Phi_{32} + G_{1133}(f_1^2 - f_3^2) \\ &\times \sin 2\Phi_{31} + 2G_{1223} f_2^2 (f_1/f_3 - f_3/f_1) - G_{1223}(4f_1 f_3 + f_2^2(f_1/f_3 + f_3/f_1)) \\ &\times \sin\Phi_{2231} + G_{1113} f_1 (f_1^2/f_3 - f_3)\sin\Phi_{31} + G_{1333} f_3 (f_1 - f_3^2/f_1)\sin\Phi_{31}\}. \end{aligned} \quad (2)$$

In Eq. (2) $\delta_j = \omega_j - \omega_{cj}$, $\Phi_{jk} = \varphi_j - \varphi_k - (\omega_j - \omega_k)t$, and $\Phi_{2231} = 2\varphi_2 - \varphi_1 - \varphi_3 - (2\omega_2 - \omega_1 - \omega_3)t$.

Phase locking $d(2\varphi_2 - \varphi_1 - \varphi_3)/dt = 0$ occurs when *three* conditions are satisfied: $f_1 \approx f_3$; the frequency locking of the hot modes $\omega_1 + \omega_3 = 2\omega_2$; the mode amplitudes are sufficiently large so that the nonlinear term on the right-hand side of Eq. (2) cancels the term $\delta_1 + \delta_3 - 2\delta_2 = 2\omega_{c2} - \omega_{c1} - \omega_{c3}$ originating from the waveguide dispersion of the cold modes. These conditions agree with the observed behavior of the amplitudes, phases, and frequencies of the transverse modes. Indeed, as one can see from Figs. 2(b) and 2(c), the lasing starts on the TM_{01} mode which has the lowest threshold [12]. With increasing current, the TM_{00} and TM_{02} modes become involved in generation and become nonlinearly coupled with the TM_{01} mode by the four-wave mixing process. Above the locking-threshold current of the order of 0.8 A, the amplitudes of the TM_{00} and TM_{02} modes become very close to each other

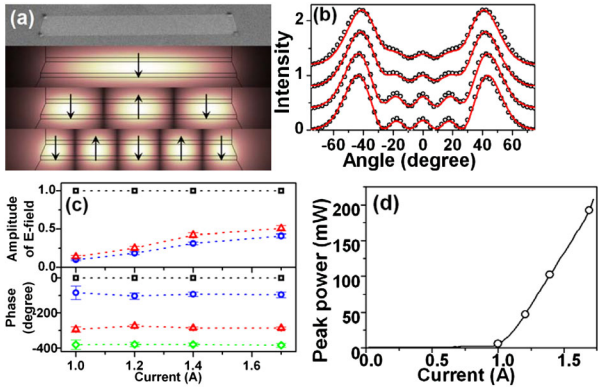

FIG. 4 (color online). (a) SEM image of the facet of a QCL with a 22-μm-wide active region, and simulations showing from top to bottom the electric field of TM_{00}, TM_{02}, and TM_{04} modes of the device; the arrows in the figure indicate the polarization of the field. (b) Measured far-field intensity distributions of the device (open circles) and their fits (solid lines) at driving currents of 1.7, 1.4, 1.2, and 1.0 A (from top to bottom). The curves are shifted vertically for clarity. (c) Electric-field amplitude (upper panel) and phase (lower panel) of the transverse modes used to fit the far-field data in (b). Open circles: TM_{00} mode; open triangles: TM_{02} mode; open squares: TM_{04} mode; open diamonds: $\phi_{TM00} + \phi_{TM02} - 2\phi_{TM04}$. Dotted lines are used to guide the eyes. Error bars indicate the range of individual parameter changes that will lead to a root mean square deviation of 0.05 between the experimental data and the fits. (d) Light output versus current curve for the device. The dots indicate the operating conditions at which the different near- and far-field measurements were performed.

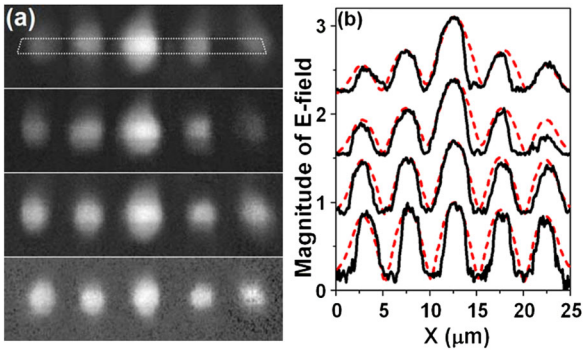

FIG. 5 (color online). (a) NSOM images of the laser modes on the facet of the 22-μm QCL at driving currents of 1.7, 1.4, 1.2, and 1.0 A (from top to bottom). Image size: 25 μm $\times$ 6.9 μm. The dashed trapezoidal frame in the first panel indicates the laser active region. (b) Line scans of the NSOM images (solid lines) and near-field mode profiles (dashed lines) calculated using the amplitudes and phases extracted from the far-field fits [Fig. 4(c)] at driving current 1.7, 1.4, 1.2, and 1.0 A (from top to bottom). The near-field mode profiles are shifted vertically for clarity.

and the phase difference $2\varphi_2 - \varphi_1 - \varphi_3$ does not change with current [Fig. 2(c) lower panel]. Furthermore, at low currents, the three peaks in the lower panel of Fig. 1(b), corresponding to three combs of the longitudinal modes, are nonequidistant because of the cold cavity dispersion. Above the locking-threshold current, the triplet of longitudinal modes belonging to three different combs are locked into the equidistant relationship $\omega_2 - \omega_1 = \omega_3 - \omega_2$. This results in three equidistant peaks in the upper panel of Fig. 1(b).

One can perform a similar analysis for 22-μm wide lasers that start lasing on the TM_{04} mode, which has the lowest threshold [12]; see Figs. 4(b) and 4(c). With increasing current, the modes TM_{00} and TM_{02} become involved in generation. Therefore, three dominant coupled transverse modes 1, 2, and 3 for these devices are TM_{00}, TM_{02}, and TM_{04} modes, respectively. We find that the process that can lead to phase locking is of the type $TM_{04} + TM_{04} \rightarrow TM_{00} + TM_{02}$, which yields a constant phase difference $2\varphi_3 - \varphi_1 - \varphi_2 = 2\pi n$, $n = 0, \pm 1, \ldots$, when $f_1 \approx f_2$, $\omega_1 + \omega_2 = 2\omega_3$, and the modal amplitudes are high enough to beat the dispersive term $\delta_1 + \delta_2 - 2\delta_3 = 2\omega_{c3} - \omega_{c1} - \omega_{c2}$. The above conditions are again in excellent agreement with observations.

In conclusion, using near-field and far-field measurements we observed phase coherence between several transverse modes in QCLs over a broad range of injection currents. Our data can be explained by phase-sensitive nonlinear coupling of transverse modes due to resonant $\chi^{(3)}$ nonlinearity of the active medium. Evidence for stable transverse mode locking was observed for all 12, 17, and 22-μm wide devices processed from the same wafer. We believe that transverse mode locking is a *universal* phenomenon for high power QCLs that support multiple low-loss transverse modes. The resulting frequency- and phase-locked multimode spectrum can be further utilized for creating various far-field radiation patterns, control of the beam quality and beam steering, and facilitating ultrashort pulse generation.

*Corresponding author.
belyanin@tamu.edu; capasso@seas.harvard.edu

[1] Y. I. Khanin, *Principles of Laser Dynamics* (Elsevier, Amsterdam, 1995).
[2] C. Y. Wang *et al.*, Phys. Rev. A **75**, 031802(R) (2007).
[3] A. Gordon *et al.*, Phys. Rev. A **77**, 053804 (2008).
[4] W. W. Bewley *et al.*, IEEE J. Quantum Electron. **41**, 833 (2005).
[5] T. L. Paoli, IEEE J. Quantum Electron. **12**, 770 (1976).
[6] M. F. C. Schemmann *et al.*, Appl. Phys. Lett. **66**, 920 (1995).
[7] G. L. Tan, R. S. Mand, and J. M. Xu, IEEE J. Quantum Electron. **33**, 1384 (1997).
[8] X. Fu *et al.*, IEEE J. Quantum Electron. **34**, 1447 (1998).
[9] J. Buus, IEEE J. Quantum Electron. **19**, 953 (1983).
[10] K. Staliunas, M. F. H. Tarroja, and C. O. Weiss, Opt. Commun. **102**, 69 (1993).
[11] M. Troccoli *et al.*, Electron. Lett. **41**, 1059 (2005).
[12] N. Yu *et al.*, Opt. Express **15**, 13227 (2007).
[13] B. Knoll and F. Keilmann, Opt. Commun. **182**, 321 (2000).